RSC Advances

ROYAL SOCIETY OF CHEMISTRY

www.rsc.org/advances

Studies on Yb-doping Effects on Photoelectrochemical Properties of WO_3 Photocatalysts

Siao Li Liew*, Gomathy Sandhya Subramanian, Chua Chin Seng, and He-Kuan Luo*

Institute of Materials Research and Engineering, Agency for Science, Technology and Research, 2 Fusionopolis Way, #08-03, Innovis, Singapore 138634

*corresponding authors

Abstract

Yb-doped WO_3 photocatalysts were prepared by co-sputtering Yb and WO_3 on FTO glass and subsequent sintering at elevated temperatures in air. Between 450 and 550 ^oC of sintering temperature, photocurrent densities of Yb-doped WO_3 photocatalysts were higher and more stable than those of the pristine WO_3 photocatalysts. The Yb-doping effects on the photoelectrochemical properties were investigated with Raman, transient absorption and electrochemical impedance spectroscopies. The results show that compared to pristine WO_3 photocatalysts, Yb-doped photocatalysts sintered at up to 550 ^oC are sub-stoichiometric WO_{3-x} due to substitution of W^{6+} cation with Yb^{3+} dopants, have shorter electron-hole recombination time and higher levels of donor densities.

Key words: Yb-doping; WO_3; Photocatalyst; Photoelectrochemical; Co-sputtering

Introduction

Tungsten trioxide (WO_3) finds many applications as photocatalysts and gas sensors owing to its intrinsic properties of visible light-responsive band gap, free carrier diffusion length and good chemical stability in aqueous media. Over the years, much effort has been made to incorporate the semiconducting metal oxides with another metal to further enhance its photoelectrochemical properties. For example, the catalytic modification of WO_3 surface by electrodeposition of Pt particles could promote the reaction rate in methanol oxidation on the photoanode, leading to significantly enhanced H_2 production efficiency compared to unmodified WO_3.[1] It is also reported that Pt-modified WO_3 films can be used as H_2 sensors which exhibited lower electrical resistances at higher Pt concentration, favouring H_2 detection possibly due to the catalytic effects of Pt clusters on the dissociative adsorption of H_2 to form H-atoms. This catalytic dissociative effect released electrons into the WO_3 matrix which in turn decreased the electrical resistance.[2] Pt nanoparticles can also be loaded onto nanoporous WO_3 nanotubes, which greatly increased photocatalytic activity because the large surface area of WO_3 nanotubes offered much more active sites in close proximity to the Pt nanoparticles to facilitate the transfer of photoelectrons to the Pt nanoparticles.[3]

To enhance the photoelectrochemical property of WO_3, the incorporations of other transition metals such as Mo, Ti and Fe were also investigated.[4-6] In $Mo_xW_{1-x}O_3$ hydrates, Mo^{6+} was preferred to W^{6+} as trapping sites for electrons.[4] Therefore the substitution of W^{6+} with Mo^{6+} cations led to red shift in the absorption edge due to the reduction of Mo^{6+} to Mo^{5+}. Hence the photoelectrochemical response of WO_3 photoanodes to visible light was enhanced together with the red shift. Doping of Ti^{4+} into WO_3 semiconductor also improved photocatalytic performance under visible light due to the change in the band structure of WO_3 caused by impurity states

between the conduction band and valence band resulting in a narrower band gap.[5] The modification of WO_3 surface with Fe^{3+} extended the absorption region and reduced charge transfer resistance, leading to increased photocurrent densities.[6] All these dopings of transition metals had a common effect of narrowing the band gap of WO_3 and extending the absorption to the visible region in the solar spectrum.

A different mechanism through harnessing the electron-rich f-orbitals of Yb dopants in WO_3 was reported for the first time in our earlier study.[7] We prepared and investigated Yb-doped WO_3 photocatalysts of varying Yb concentrations for photoelectrochemical water splitting. For a Yb doping concentration as low as 0.34 at.% determined by x-ray photoelectron spectroscopy, an evident enhancement in photocurrent density was observed, which was attributed to the increased conductive carrier paths caused by oxygen vacancies and the $4f^{13}$ orbital configuration of Yb^{3+} doped into WO_3. However, a higher concentration of 1.6 at.% increased the charge transfer resistance with reduced photocurrent density compared to the pristine WO_3 possibly due to the distortion of WO_3 crystal structure induced by the larger ionic radius of Yb^{3+} relative to W^{6+}. Notwithstanding the limiting factor of the size of Yb^{3+} dopant cations, the study showed that tapping on the electron-rich f-orbitals of the lanthanide proved to be an effective means to increase the charge carrier generation for enhanced photocurrent densities in WO_3.

In order to obtain a deeper and better understanding of Yb-doped WO_3 photocatalysts for practical applications, herein we studied the Yb-doping effects at varying sintering temperatures on the photoelectrochemical properties. The results showed that Yb doping enlarged the thermal envelope of WO_3. Specifically, photocurrent densities of Yb-doped WO_3 were sustained up to 550 ^oC. However for the pristine WO_3 photocatalysts, the photocurrent density continually decreased with increasing sintering temperatures over the same range. These improvements

were evaluated in the light of structural properties, charge dynamics and donor densities of thermally treated photocatalysts investigated with Raman, transient absorption and electrochemical impedance spectroscopies. Yb-doped WO_3 photocatalysts sintered at up to 550 ^oC were sub-stoichiometric due to substitution of W^{6+} with Yb^{3+} dopants and showed shorter electron-hole recombination time but higher donor densities compared to the pristine WO_3 photocatalysts. The Yb-doping effect led to more stable and higher photocurrent densities with lower charge transfer resistances in PEC water splitting with Yb-doped WO_3 photocatalysts.

Experimental Details

Deposition

WO_3 and Yb were co-sputtered onto ultrasonically cleaned FTO glass substrates inside a magnetron sputtering chamber when the base pressure reached ~10^{-7} Torr. The sputtering power was set at 100 W and 5 W respectively for WO_3 and Yb to yield as-deposit film thickness ~450 nm. The sputtered samples were sintered in air in a box furnace at temperature range between 400 and 600 ^oC for 1 hour. A set of pristine WO_3 samples (without Yb) was also prepared using the same process parameters.

Characterisations

Structural analyses were carried out with WITec alpha 300R microscope system using 532 nm Nd YAG laser of ~1 mW power to obtain Raman spectra of the samples. Spectroscopy for each sample was averaged at 1 μm per pixel and 0.1 s per point from a 100x100 μm scan area at 100x objective. Transient absorption spectroscopy was carried out with a Nd:YAG laser (1 mJ, 7 ns, 10 Hz, 355 nm excitation) as the pump source and a 450W Xenon arc lamp as the probe source. Each spectral curve is the average of 256 measurements while each kinetics decay curve

is the average of four measurements at 16 laser shots per measurement. Secondary ion mass spectroscopy (SIMS) using ION SIMS IV to profile the distribution of Yb in WO_3 and optical absorbance measured with Shimadzu UV-3101 PC scanning spectrophotometer were carried out to supplement the spectroscopic results.

Photoelectrochemical (PEC) Measurements and Detection of Gases (H_2 and O_2)

PEC measurements were carried out in a custom-made two-compartment glass cell with a three-electrode configuration. A Pt wire as the counter electrode was placed in one compartment, separated from a Ag/AgCl reference electrode and the working electrode (sputter-deposited WO_3 on FTO substrate) in another compartment. 400 mL of Na_2SO_4 (0.05M, pH ~5.4) electrolyte solution prior purged with Ar was added to the glass cell. Current-voltage measurements under dark and illuminated conditions at scan rate 100 mV/s between -0.1 and 1.6 V Ag/AgCl were controlled by a potentiostat (Autolab PGSTAT101) connected to Nova 1.8 software. For illuminated measurements, a Xenon light source (Hamamastu LC8) with a radiant spectrum that resembles the visible portion of solar spectrum was directed at the working electrode through a quartz window in the PEC glass cell. The intensity of light was prior adjusted to 100 mW/cm^2 based on the output reading of a calibrated Si solar cell. The illuminated area on the working electrode measured ~1.5 cm by 1.0 cm. Electrochemical impedance spectroscopy was also performed using the same test cell set-up to obtain Nyquist and Mott-Schottky plots to determine charge transfer resistance and donor density respectively. For Nyquist plots, the cell was illuminated and maintained at constant bias voltages superimposed with a sinusoidal voltage 10 mV in the frequency range between 0.1 Hz and 10 kHz. For Mott-Schottky plots, measurements were made in the dark at selected frequencies between bias voltage -0.2 and 1.3 V Ag/AgCl.

A custom-built photocatalytic reactor comprising a photoelectrochemical cell and a gas chromatograph was used to simultaneously measure photocurrents and quantify gaseous products from water splitting. The cell was an 820 cm^3 glass vessel configured with a two-electrode set-up consisting of a Pt counter electrode and the sputter-deposited WO_3 working electrode. During photoelectrochemical measurement, WO_3 photocatalyst inside the cell was illuminated with a light intensity of 50 mW/cm^2 from a 150W Xenon arc lamp fitted with AM1.5 filter. A constant 1.5V bias voltage was applied through a potentiostat to the counter electrode during measurements. ~220 mL of the same electrolyte as used in the prior section was used in this testing. The gases from the photoelectrochemical cell were delivered by high purity Ar carrier gas to a gas chromatograph GC-2014 Shimadzu for analyses.

Results and Discussions

Structural Analyses

At 400 ^oC of sintering temperature, both Yb-doped and pristine WO_3 samples displayed broad Raman spectra with weak band region around wavenumber 200 cm^{-1} and a peak at 270 cm^{-1} shown in Fig. 1. The band region evolved into peaks at 130, 190 and 117 cm^{-1} and new peaks appeared at 706 and 809 cm^{-1} when the sintering temperature was increased to 450 ^oC and beyond. All the peaks which increased in intensities and sharpness with increased sintering temperatures, clearly identified both Yb-doped and pristine photocatalysts to be monoclinic WO_3 with peaks at the 200 cm^{-1} band region ascribed to lattice vibration, 270 cm^{-1} to bending and 706 - 809 cm^{-1} to stretching vibrations of W-O bonds in monoclinic WO_3.[8,9] At sintering temperatures 500 ^oC and above, Raman peaks of Yb-doped WO_3 appeared weaker than those of the pristine counterpart with clear differences observed at 550 and 600 ^oC for all the peak

regions. In addition, Yb-doping also caused a minor shift of ~2 cm^{-1} to the lower bond energies as shown by the inset graph which indicates a less ordered crystal lattice in the Yb-doped WO_3 compared to the pristine WO_3.

Distribution of Yb

The elemental depth profiling of Yb-doped WO_3 samples with SIMS (see Fig. S1a) showed that Yb distribution followed those of W and O, indicating that Yb was uniformly incorporated into the WO_3 lattice. The average composition of the Yb-doped samples was $WYb_{0.025}O_{3-x}$ from elemental analyses using an Oxford INCA x-ray energy dispersive spectrometer (EDS). The Raman and SIMS results in combination showed that very likely Yb^{3+} dopants substituted W^{6+} in the crystal lattice to form sub-stoichiometric WO_{3-x} which would be less crystalline than pristine WO_3.[10] This is in agreement with the colour change from pale green in the pristine WO_3 to deep blue in Yb-doped WO_3 as displayed by the samples shown in Fig. S1b.

Carrier Lifetime

The effect of Yb-doping on carrier transport was probed by transient absorption (TA) spectroscopic measurements. Fig. 2a shows the TA spectra obtained for spectral range between 300 and 650 nm for WO_3 photocatalysts and FTO substrate, recorded after 100 ns delay upon excitation by 355 nm laser. Strong TA signals with maxima (at ~352 to 357 nm region) were registered for both Yb-doped and pristine WO_3 with Yb-doped WO_3 exhibiting a lower signal level and a blue shift relative to the pristine WO_3. TA spectra with maxima in the UV-visible region have been ascribed to absorption by photoholes in metal oxides such as Fe_2O_3, WO_3, TiO_2 and $BiVO_4$.[11-14] A lower TA signal for Yb-doped WO_3 would infer fewer photoholes were probed in the spectra range due possibly to faster recombination of electrons and holes in the less ordered crystal lattice. The blue shift observation corroborates with the optical absorption

spectra in Fig. S2 which shows that Yb doping did not produce the desired red shifts of the absorption edges of WO_3 for all the sintering temperatures, unlike the reported doping effects of Mo, Ti and Fe transition metals into WO_3 semiconductor where the band gap was narrowed and the absorption region was extended to the visible range of solar spectrum (i.e. red shift).[4-6] Both the TA and optical absorption spectra in this present study suggested the presence of Yb oxides with wide band gaps in the Yb-doped WO_3 probably contributed to the non-red shifts in the absorption edges. Fig. 2b shows the decay kinetics of TA probed at 400 nm wavelength revealed a rapid decrease in the TA signals for the first 10 ms followed by a gradual decrease up to 0.1 s for both Yb-doped and pristine photocatalysts, which resembles the occurrence of bulk recombination of electrons and holes in semiconductor photocatalysts for similar excitation conditions.[11,13,15] However the reported recombination times $t_{1/2}$ (time to reach half of the initial concentration of charge carriers) of these photocatalysts were usually in the order of microseconds. In the present study with no bias voltage applied, $t_{1/2}$ for both Yb-doped and pristine WO_3 samples were higher than the literature values[11,13,15] with Yb-doped WO_3 having a shorter $t_{1/2}$ of ~0.46 ms compared to 0.87 ms for the pristine WO_3. $t_{1/2}$ of Yb-doped WO_3 shows that the mobility of free carriers in the doped photocatalyst was not severely impaired by the doping of Yb even though Raman spectroscopic measurements indicated the crystal lattice was less ordered in the Yb-doped WO_3 compared to the pristine WO_3. The long recombination time in WO_3 is linked to its free carrier diffusion length which can be up to two orders of magnitude higher than that of either TiO_2 or Fe_2O_3. Long carrier lifetime is desired in photocatalytic applications for increased free electron-hole pairs to enhance photocurrents although it does not necessarily lead to increased photocurrents.

Photoelectrochemical (PEC) Studies

The photocurrent densities and electrochemical impedances from PEC testing are plotted in Fig. 3. Between 450 and 550 ^{o}C of sintering temperatures, photocurrent densities of Yb-doped WO_3 photocatalysts were both fairly constant and higher than for pristine WO_3. However, the photocurrents of Yb-doped WO_3 photocatalysts sintered at 400 and 600 ^{o}C were low. The charge transfer resistance values corresponded to the photocurrent densities albeit in opposite trend. Fig. 3c summarises the contrasting effects of sintering temperatures from 450 to 550 ^{o}C (at 1.2 V Ag/AgCl) for Yb-doped WO_3 which maintained constant levels of 1.2 mA/cm^2 (corresponding to 525 to 626 Ω) and for pristine WO_3 which displayed decreasing levels from 1.0 to 0.4 mA/cm^2 (corresponding to 710 to 1300 Ω).

To further investigate the effects of Yb-doping on photocurrents, electrochemical impedance spectroscopy (EIS) measurement for each photocatalyst was carried out in the dark at 1000 Hz between -0.2 and 1.4 V to obtain capacitance values which were fitted to Mott–Schottky (MS) equation as shown in Fig. 4. Except for samples sintered at 400 and 600 ^{o}C, the slope of each MS plot which equals to $\frac{2}{e\varepsilon\varepsilon_o N_D}$, was significantly lower for Yb-doped WO_3 compared to pristine WO_3, in other words doping resulted in increased donor densities. (Note: e is the electron charge, ε is dielectric constant of WO_3 (50), ε_o is permittivity of vacuum, N_D is donor density).[16] As Yb was co-sputtered at the same sputtering power for all the doped samples, it is expected that N_D will be similar for all the doped samples regardless of the sintering temperatures. As shown in Fig. 4b, the N_D values ranged from 2.92x10^{20} to 6.33x10^{20} cm^{-3} for Yb-doped WO_3 versus a lower level of 6.08x10^{19} to 1.98x10^{20} cm^{-3} for pristine WO_3 for sintering temperatures between450 and 550 ^{o}C. The N_D values for both doped and pristine WO_3 were however low at

the extreme temperatures (400 and 600 ^{o}C) when compared to the respective N_D values for 450 to 550 ^{o}C range.

Thus far, it has been shown that Yb-doped WO_3 photocatalysts demonstrated photocurrent enhancement with reduced charge transfer resistances. Raman spectroscopy and SIMS results (Fig. 1 and Fig. S1) showed that Yb^{3+} dopants substituted W^{6+} in the crystal lattice which would have resulted in oxygen vacancies to form sub-stoichiometric WO_{3-x}. Oxygen vacancies created in PO_4 salts had been reported to widen the valence band and thus narrow the band gap to yield enhanced photoactivity.[17,18] However in the present study, blue shift (hence no narrowing of band gap) was observed in the transient absorption spectra instead (Fig. 2) which more probably reflects the presence of Yb oxides with wide band gaps. Besides, the carrier life time of Yb-doped WO_3 was shorter than that of pristine WO_3. The enhanced photocatalytic activity of Yb-doped WO_3 is attributed to increased donor densities as shown by Mott–Schottky plots in Fig. 4. The electrons available from the 4f and 6s orbitals of Yb and the shallow electron donors from oxygen vacancies[19] arising from substitution of W by Yb contributed to a higher electron density for the doped WO_3. Even at increased sintering temperatures where an amorphous layer formed at the WO_3/electrolyte interface would thicken[20], the higher electron density would enable more free electrons to tunnel through to result in reduced charge transfer resistances and hence increased photocurrent densities. The higher electron density effect was sustained up to 550 ^{o}C of sintering temperature as indicated by the stabilities of photocurrent densities and electrochemical impedances of Yb-doped WO_3 shown in Fig. 3c. In contrast, a lower electron density in the pristine WO_3 would be impeded by the amorphous layer formed at the WO_3/electrolyte interface and led to decreasing photocurrents and increasing electrochemical impedances over the same sintering temperature range. However at the extreme sintering

temperatures of 400 and 600 ^{o}C, photocurrent densities of both Yb-doped and pristine WO_3 were lower as shown in Fig. 3(c) which corresponded to the decreased electron density levels shown in Fig. 4. At 400 ^{o}C, both doped and pristine WO_3 were not fully crystallised as indicated by the broad Raman spectra in Fig. 1(a) which would imply presence of grain boundaries to trap free electrons. On the other hand at 600 ^{o}C, although crystallinities of both doped and pristine WO_3 increased as shown by the sharp peaks in the Raman spectra in Fig. 1(e), amorphous layer formed at the photocatalyst/electrolyte interface by oxidation[20] could have altered the effective dielectric constants of the photocatalysts and lowered the capacitance values and the free donor carrier densities. While the present study shows that doping a small amount of electron-rich Yb can increase donor densities and lead to higher PEC photocurrent densities, increasing the doping level of Yb into WO_3 continuously may nullify the benefits of increasing donor density due to distortion of WO_3 crystal structure which impeded charge transport and increased the charge transfer resistance as reported in our earlier study.[7]

To confirm that the photocurrents of Yb-doped and pristine WO_3 photocatalysts sputtered-deposited in this study were due to photoelectrochemical reaction of water, water splitting products (H_2 and O_2) were collected and analysed with the in-house photocatalytic reactor coupled with a gas chromatograph. H_2 gas was detected at every hour interval as shown in the gas evolution plot in Fig. 5 although O_2 gas was not so conclusively identified during the first half of the reaction (~3 hours), probably due to the lower amount produced and higher solubility in water. Electrolysis in the dark with the same photocatalyst was also carried out to verify that no gaseous products were collected without light irradiation. 1.46 μmol of H_2 was collected at the end of six hours of photocatalytic reaction for Yb-doped WO_3. Given that the surface area of photocatalyst was 1.5x1.0 cm^2, the H_2 yield was ~2000 $\mu mol.h^{-1}.m^{-2}$ which was considerably

lower than those reported for WO_3 nanostructures.[21-23] Yet high photo-stability was demonstrated with only ~10% drop in photocurrent at the end of 6 hours of photocatalysis shown in Fig. S3.

Conclusions

We prepared Yb-doped WO_3 photocatalysts by co-sputtering of Yb and WO_3 and subsequent sintering at elevated temperatures in air from 400 to 600 ^oC. The Yb-doping effects on photoelectrochemical (PEC) properties were investigated with Raman, transient absorption and electrochemical impedance spectroscopies. Raman spectroscopic investigations showed that the intensities of lattice vibration and vibration of W-O bonds in monoclinic WO_3 were reduced for Yb-doped WO_3 relative to pristine WO_3, which is due to substitution of W^{6+} by Yb^{3+} dopants to form sub-stoichiometric WO_{3-x}. Transient absorption (TA) spectroscopy showed lower TA signals for Yb-doped WO_3 relative to the pristine WO_3. The recombination time of electrons and holes in Yb-doped WO_3 was shorter than that of the pristine WO_3. The electrochemical impedance spectra revealed higher levels of donor densities for Yb-doped WO_3. The Yb doping effect led to more stable and higher photocurrent densities with lower charge transfer resistances in PEC water splitting with Yb-doped WO_3 photocatalysts sintered between 450 and 550 ^oC. In contrast, photocurrent densities of the pristine WO_3 decreased steadily with increased charge transfer resistances.

Acknowledgement

This work was supported by the Institute of Materials Research and Engineering (IMRE), Agency for Science, Technology and Research (A*STAR) (Grant code: IMRE/12-1C0101).

References

1 D. V. Esposito, J. G. Chen, R. W. Birkmire, Y. Chang and N. Gaillard, *Int. J. Hydrogen Energy*, 2011, **36**, 9632-44.

2 C. Zhang, A. Boudiba, C. Navio, C. Bittencourt, M-G. Olivier, R. Snyders and M. Debliquy, *Int. J. Hydrogen Energy,* 2011, **36**, 1107-14.

3 Z. Zhao and M. Miyauchi, *Angewandte Chemie, Int. Ed.*, 2008, **47**, 7051 –7055.

4 L. Zhou, J. Zhu, M. Yu, X. Huang, Z. Li, Y. Wang and C. Yu, *J. Phys. Chem. C,* 2010, **114**, 20947-54.

5 C. Feng, S. Wang, and B. Geng, *Nanoscale*, 2011, **3**, 3695-9.

6 S. Han, J. Li, X. Chen, Y. Huang, C. Liu, Y. Yang and W. Li, *Int. J. Hydrogen Energy*, 2012, **36**, 4724-31.

7 S. L. Liew, Z. Zhang, T. W. Glenn Goh, G. S. Subramanian, H. L. Debbie Seng, T. S. Andy Hor, H.-K. Luo and D. Z. Chi, *Int. J. Hydrogen Energy*, 2014, **39**, 4291-98.

8 M. F. Daniel, B. Desbat and J. C. Lassegues, *Journal of Solid State Chemistry*, 1987, **67**, 235-247.

9 C. V. Ramana, S. Utsunomiya, R. C. Ewing, C. M. Julien and U. Becker, *J. Phys. Chem. B,* 2006, **110**, 10430-11035.

10 G. Wang, Y. Ling, H. Wang, X. Yang, C. Wang, J. Z. Zhang and Y. Li, *Energy and Environmental Science*, 2012, **5**, 6180-7.

11 S. R. Pendlebury, M. Barroso, A. J. Cowan, K. Sivula, J. Tang, M. Grätzel, D. Klug and J. R. Durrant, *Chemical Communications,* 2011, **47**, 716–718.

12 F. M. Pesci, A. J. Cowan, B. D. Alexander, J. R. Durrant and D. R. Klug, *J. Phys. Chem. Lett.*, 2011, **2**, 1900–1903.

13 T. Yoshihara, R. Katoh, A. Furube, Y. Tamaki, M. Murai, K. Hara, S. Murata, H. Arakawa and M. Tachiya, *J. Phys. Chem. B*, 2004, **108**, 3817-3823.

14 Y. Ma, S. R. Pendlebury, A. Reynal, F. Le Formal and J. R. Durrant, *Chemical Science*, 2014, **5**, 2964–2973.

15 J. Tang, J. R. Durrant and D. R. Klug, *J. Phys. Chem. B*, 2004, **108**, 3817-3823.

16 M. A. Butler, *Journal of Applied Physcis*, 1977, **48**,1914-20.

17 Y. Lv, Y. Zhu and Y. Zhu, *J. Phys. Chem. C*, 2013, **117** (36), 18520–18528.

18 L. J. Chen, Y. J. Zhao, J. Y. Luo, Y. Y. Xia, *Phys. Lett. A*, 2011, **375**, 934−938.

19 S. K. Deb, *Phys. Rev. B: Condens. Matter Mater. Phys.*, 1977, **16**, 1020–1024.

20 F. Lin, C. P. Li, G. Chen, R. C. Tenent, C. A. Wolden, D. T. Gillaspie, A. C. Dillon, R. M. Richards and C. Engtrakul, *Nanotechnology*, 2012, **23**, 255601 (8pp).

21 C. W. Lai and S. Sreekantan, *Int. J. Hydrogen Energy*, 2013, **38**, 2156-66.

22 J. Lin, P. Hu, Y. Zhang, M. Fan, Z. He, C. K. Ngaw, J. S. C. Loo, D. Liao and T. T. Y. Tan, *RSC Advances*, 2013, **3**, 9330-9336.

23 Q. Chen, J. Li, B. Zhou, M. Long, H. Chen, Y. Liu, M. Long, W. Cai and W. Shangguan, *Electrochem. Commun.*, 2012, **20**, 153-156.

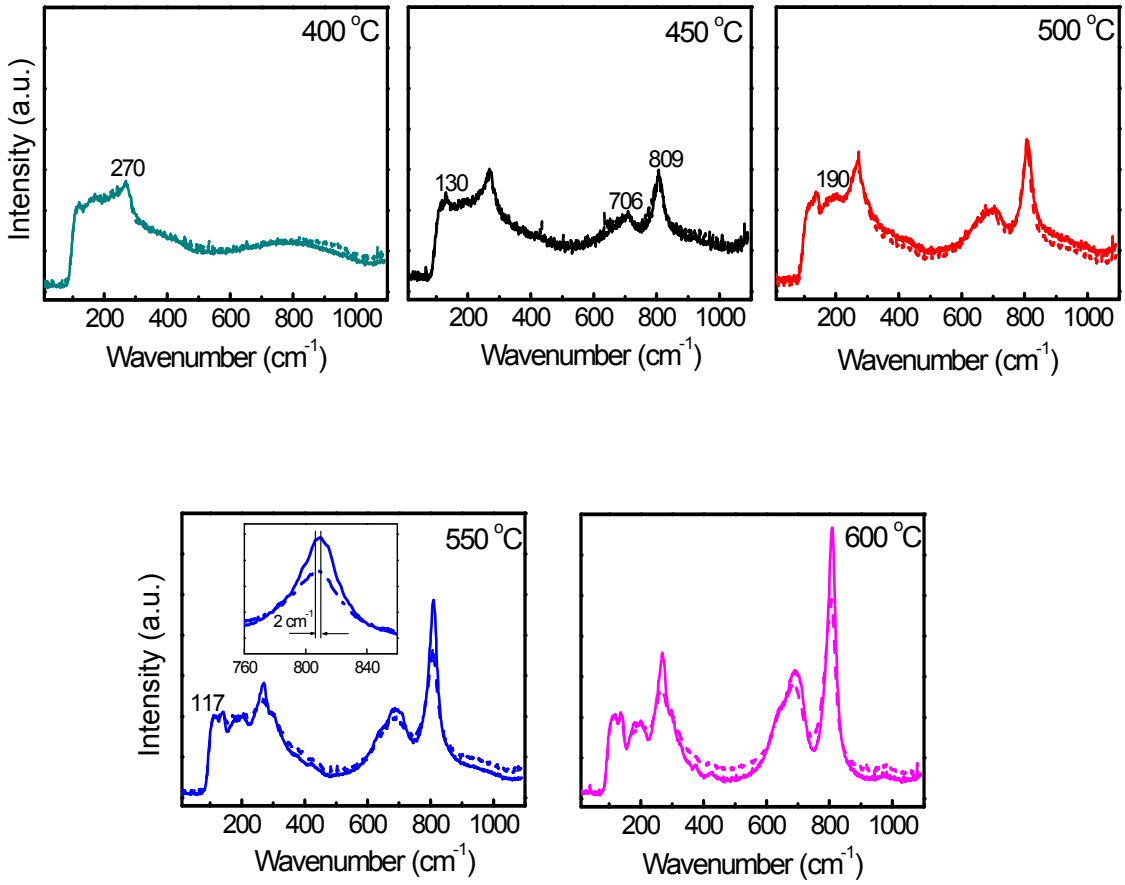

Fig. 1 Raman spectra of Yb-doped (dashed lines) and pristine (solid lines) WO_3 sintered from 400 to 600 ^{o}C. Peak indexing is for the first appearance of the peak. The inset spectrum at 550 ^{o}C shows blue shift in Raman peak at 809 cm^{-1} of doped WO_3 by ~2 cm^{-1}.

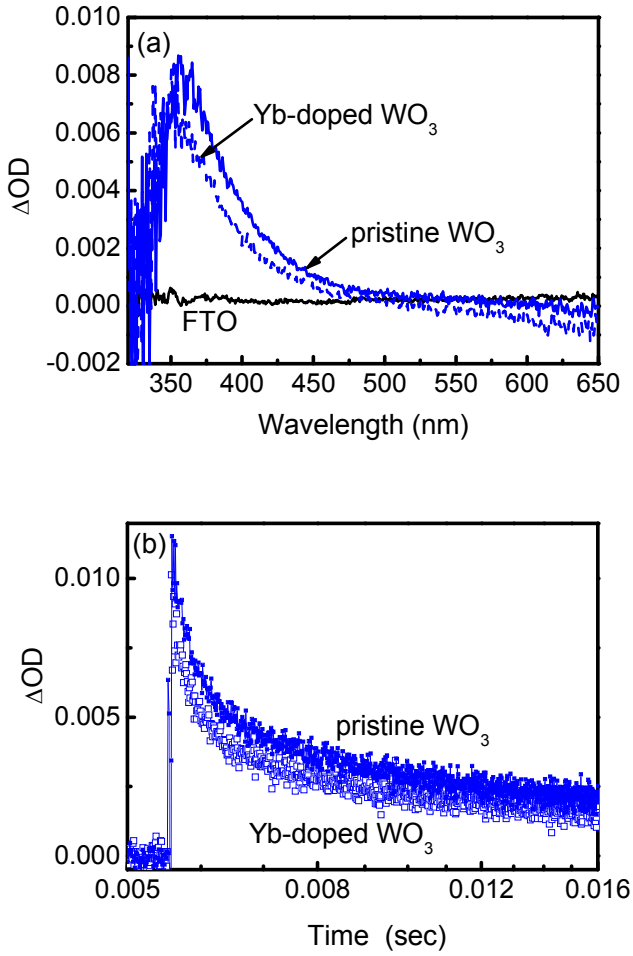

Fig. 2(a) Transient absorption spectra of Yb-doped and pristine WO_3 sintered at 550 ^{o}C. Bare FTO substrate was also measured as a reference. The spectra were measured at 100 ns delay after excitation by 355 nm laser. (b) Transient kinetic decays of Yb-doped and pristine WO_3 probed at 400 nm.

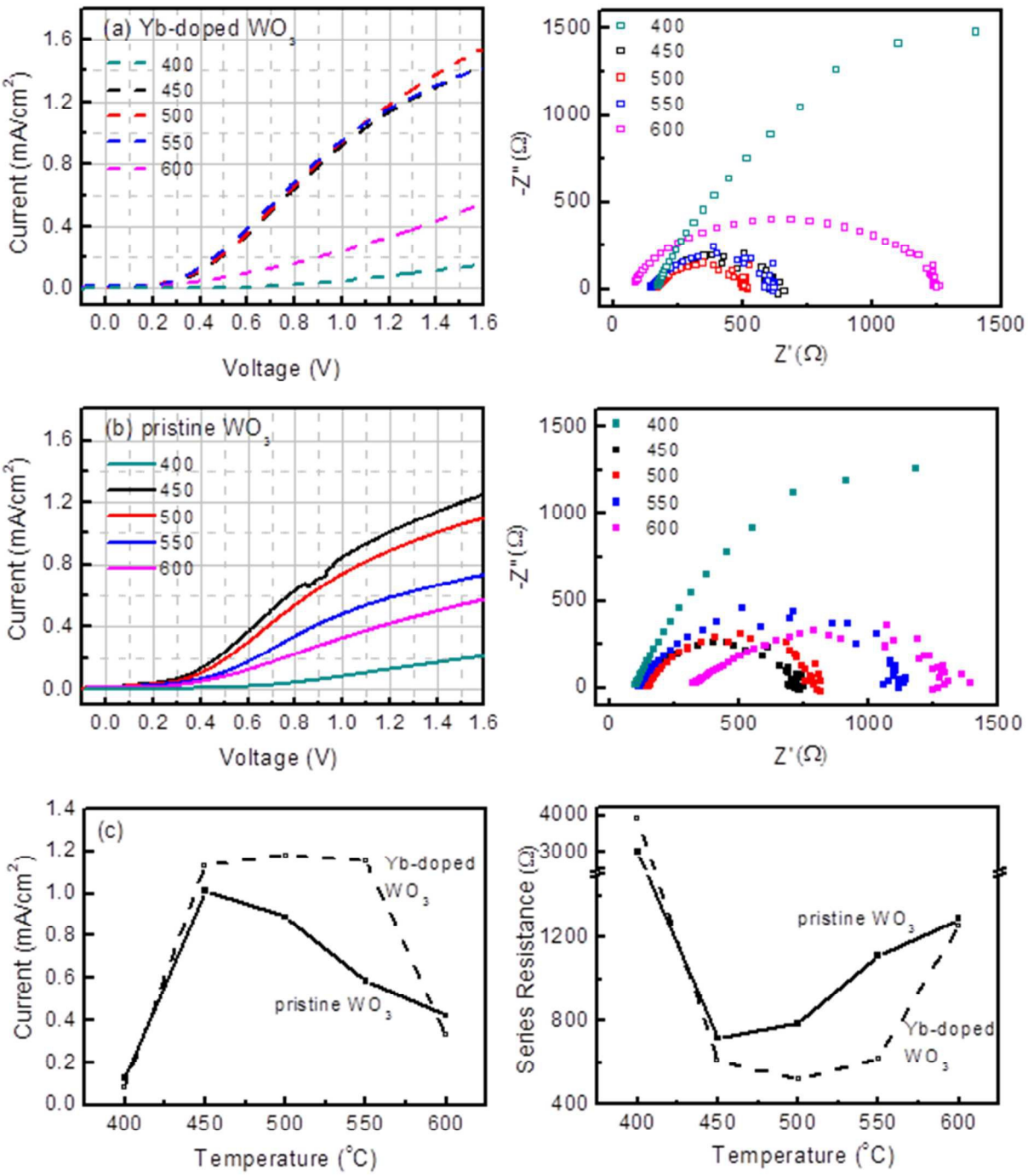

Fig. 3 Photoelectrochemical testings of Yb-doped and pristine WO_3 sintered at different temperatures. Photocurrent densities versus voltage (left) and electrochemical impedances (right, at constant bias voltage 1.2V and illuminated) for (a) Yb-doped WO_3 and (b) pristine WO_3. (c) Effects of sintering temperatures on photocurrent densities and series resistances.

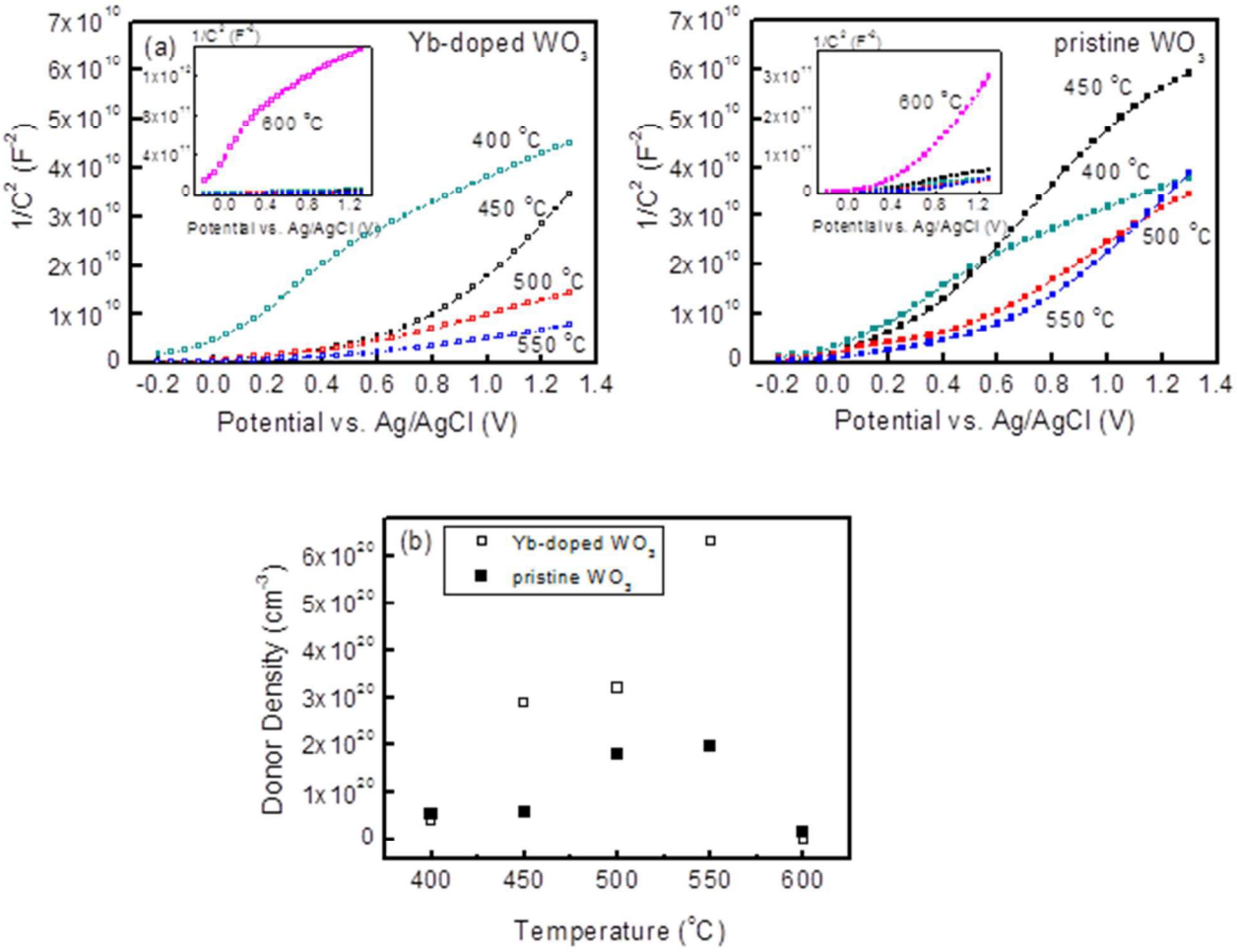

Fig. 4 Electrochemical impedance spectroscopy in dark condition for Yb-doped and pristine WO_3 sintered at different temperatures. (a) Mott–Schottky plots to derive donor densities. The insets include plots for samples sintered at 600 ^{o}C. (b) Effects of sintering temperatures on donor densities.

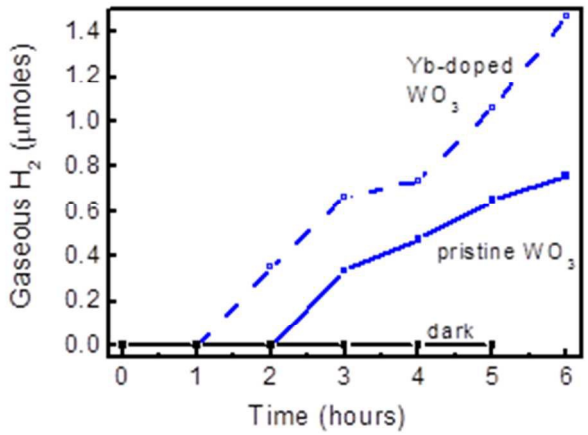

Fig. 5 Gaseous H_2 evolution from Yb-doped and pristine WO_3 during photoelectrochemical water splitting. Electroylsis in the dark was also carried out to verify that no gaseous products were collected without light irradiation.